Continuous Improvement of H-Mode Discharge Performance with Progressively Increasing Lithium Coatings in the National Spherical Torus Experiment

R. Maingi,[1] S. M. Kaye,[2] C. H. Skinner,[2] D. P. Boyle,[3] J. M. Canik,[1] M. G. Bell,[2] R. E. Bell,[2] T. K. Gray,[1] M. A. Jaworski,[2] R. Kaita,[2] H. W. Kugel,[2] B. P. LeBlanc,[2] D. K. Mansfield,[2] T. H. Osborne,[4] S. A. Sabbagh,[5] and V. A. Soukhanovskii[6]

[1]*Oak Ridge National Laboratory, Oak Ridge, Tennessee 37831, USA*
[2]*Princeton Plasma Physics Laboratory, PO Box 451, Princeton, New Jersey 08543, USA*
[3]*Princeton University, Princeton, New Jersey 08543, USA*
[4]*General Atomics, San Diego, California 92186, USA*
[5]*Columbia University, New York, New York 10027, USA*
[6]*Lawrence Livermore National Laboratory, Livermore, California 94550, USA*

(Received 3 June 2011; published 29 September 2011)

Lithium wall coatings have been shown to reduce recycling, improve energy confinement, and suppress edge localized modes in the National Spherical Torus Experiment. Here, we show that these effects depend continuously on the amount of predischarge lithium evaporation. We observed a nearly monotonic reduction in recycling, decrease in electron transport, and modification of the edge profiles and stability with increasing lithium. These correlations challenge basic expectations, given that even the smallest coatings exceeded that needed for a nominal thickness of the order of the implantation range.

DOI: 10.1103/PhysRevLett.107.145004 PACS numbers: 52.40.Hf, 52.25.-b, 52.30.-q, 52.55.-s

Low-Z wall conditioning has been employed [1] in fusion devices for many years to improve plasma performance and manage the intense plasma-wall interactions. Recently, there is growing use of lithium coatings, in particular, to control edge recycling and improve energy confinement [2–6]. The basic concept is to coat the plasma-facing components with tens of atomic monolayers of low-Z elements, reducing higher-Z impurity generation and influx, which detracts from plasma performance. Deuterium pumping takes place in an implantation layer that increases with the incident ion energy (E_i) up to 100–200 nm deep [7] for $E_i \leq 2$ keV. These original calculations were based on divertor electron temperature $T_e \sim 420$ eV; in fact, the maximum divertor T_e from Langmuir probe measurements in the National Spherical Torus Experiment (NSTX) is 30–40 eV, with an expected $E_i \leq 200$ eV and a corresponding range ≤ 10 nm. In this simple picture, coatings thicker than this should not improve performance; on the contrary, thick coatings could form macroscopic flakes, which could lead to disruptions if mobilized.

Here, we present new analysis for a controlled sequence of progressively increasing lithium coatings, demonstrating for the first time the continuous improvement of a number of discharge characteristics with increasing coatings, all with nominal thickness $\gg 10$ nm. While discrepancies between new experiments and predictions are not uncommon, theses results are particularly relevant because the disagreement is very favorable for fusion research. Specifically, the improvement in energy confinement (τ_E) translates to smaller device size to achieve the same core performance goals, and the broadening of the pressure profile leads to higher magnetohydrodynamic (MHD) stability limits. Note that the word ''coatings'' above is not intended to imply a pure lithium layer; indeed, spectroscopic emission shows that the surface consists of a mixed material.

The remainder of this Letter is organized as follows. We first describe the discharge sequence with increasing coatings, showing how plasma parameters changed nearly continuously as lithium was increased. Next, we document the gradual reduction in electron transport over the outer half of the plasma minor radius with increasing wall coatings. Then, we show that the nearly monotonic progression toward edge localized mode (ELM) suppression with increasing lithium can be understood in the context of an apparent threshold in the edge electron density and pressure profile characteristic widths. Finally, we summarize these results.

Lithium was first introduced into the NSTX in 2005 via pellet injection, with modest, short-lived effects on the discharge characteristics [8]. A lithium evaporator (LiTER) was installed in 2007 to coat the lower portion of the NSTX between discharges; this resulted in reduced recycling, improved τ_E, and a reduction of edge instabilities known as ELMs [9]. In 2008, a second LiTER was installed into NSTX to provide 360° coverage of the lower divertor, thereby reducing shadowed regions [10,11]. Lithium from the previous campaign's experiments had been removed by surface abrasion of the tiles during the vent prior to the operations. Dedicated experiments using periodic boronization of the graphite plasma-facing components were used for approximately a month to provide reproducible ELMy H-modes. The lithium was then introduced gradually but systematically, to document its impact on global discharge characteristics, plasma profiles, and

ELM activity. Preliminary analysis of the ELM characteristics is published elsewhere [12], as is detailed stability analysis [13] of the edge profiles for the ELMy discharges without lithium and the ELM-free discharges with lithium.

A reference NSTX scenario with ordinary type I ELMs was developed several years ago in an Alcator C-Mod–MAST–NSTX similarity experiment [14] on small ELM regimes. These ELMs individually cause a fractional stored energy drop $\Delta W/W \sim 2$–5%, with a nominal frequency of $\sim$100 Hz that increased with heating power. There are no small, type V ELMs in this discharge scenario, which are otherwise common [15] in NSTX. Other relevant discharge parameters were $I_p = 0.8$ MA, $B_t = 0.45$ T, $P_{\mathrm{NBI}} = 4$ MW, and line-average electron density n_e from 4–6.5 $\times 10^{19}$ m^{-3}. Periodic boronizations in the run campaign had been applied prior to this experiment.

Lithium was introduced methodically into the ELMy H-mode discharge scenario described above. Helium glow discharge cleaning of 6.5 min duration was used between all of the discharges, followed by lithium evaporation with diagnostic window shutters closed. During the plasma discharges, a LiTER shutter was used to prevent lithium evaporation into the vacuum vessel to avoid coating of the diagnostic windows. Figure 1 shows the lithium deposition between discharges during the sequence, as well as the cumulative deposition. The deposition rate was kept roughly constant between the first 9 discharges and was gradually increased afterwards. The minimum lithium evaporation was 110 mg, corresponding to a nominal film thickness between 30 and 125 nm in the divertor region [11]. We emphasize that this sequence was the first use of lithium in this campaign, ensuring no lithium was present in the reference discharges. The gas fueling, neutral beam input power P_{NBI}, and boundary shape were held constant until the very end of the scan, when higher fueling and lower P_{NBI} were needed to avoid MHD instabilities.

The evolution of other relevant plasma parameters during the scan is shown in Fig. 2. Panel (a) shows that the lower divertor D_α emission, indicative of recycling, gradually decreased with increasing lithium coatings. The line-average density was also gradually reduced, while the peak plasma stored energy W_{MHD} (occurring generally between 0.45 and 0.6 sec) from equilibrium reconstructions [16] gradually increased (not shown). Panel (b) shows that the τ_E derived from W_{MHD} and normalized by the ITER-97 L-mode global scaling [17] increased slowly during the scan, showing no clear sign of saturation with increasing lithium, i.e., even in the ELM-free regime (five of the six discharges in panel (b) with evaporation >200 mg were ELM-free). Panels (c), (d), and (e) show that peaking of the electron kinetic profiles was correlated with the amount of predischarge lithium deposition. The n_e peaking factor initially increased as the lithium deposition was increased; this is due to a general reduction in the edge density. As the discharges became nearly ELM-free, the density profile became more hollow, leading to a reduced peaking factor with >300 mg predischarge lithium. On the other hand, the T_e and electron pressure, P_e, profiles' peaking factors decreased nearly monotonically with increasing lithium deposition. Note that we previously reported a reduction in the peaking factor for "standard" discharges with a fixed predischarge lithium coating [10]. In contrast, the ion profile peaking factors did not show a clear trend during the scan.

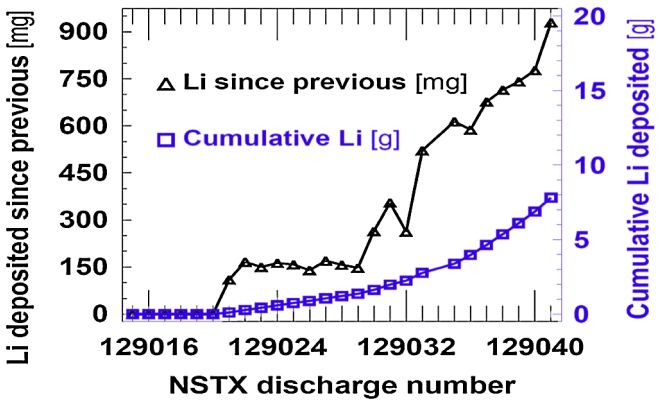

FIG. 1 (color online). Lithium deposition during the systematic experiment: "fresh" lithium before the discharge in triangles and cumulative lithium coating in squares.

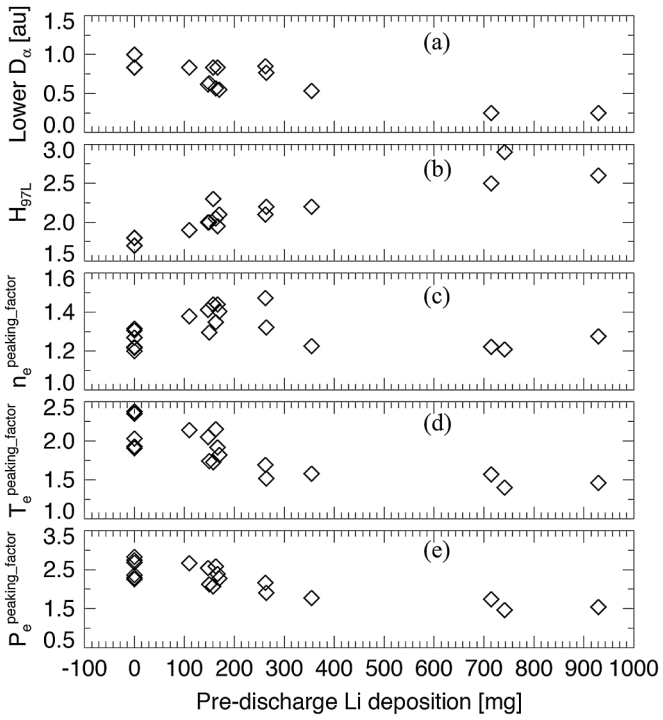

FIG. 2. Evolution of plasma parameters as a function of predischarge lithium evaporation: (a) Lower divertor D_α baseline value at $t = 0.4$ sec, (b) energy confinement relative to ITER97-L scaling, (c) n_e profile peaking factor, (d) T_e profile peaking factor, and (e) P_e profile peaking factor. Panels (b)–(e) were computed at the time of peak W_{MHD}.

The core transport during this scan was evaluated (Fig. 3) at the time of peak W_{MHD} with the TRANSP code [18], using kinetic data and reconstructed equilibria from the EFIT code [16,19]. Panel (a) shows that both the total and electron τ_E increased with increasing lithium deposition; indeed, the electron τ_E increased more rapidly than the global τ_E. Panel (b) shows that the core electron and ion thermal diffusivities χ_e and χ_i near the core at $r/a = 0.35$ were insensitive to or weakly increasing with the predischarge lithium deposition. In contrast, the edge χ_e at $r/a = 0.7$ decreased strongly with increasing lithium deposition [panel (c)]; however, the ion thermal diffusivity χ_i actually increased modestly. It is clear that the changes in the edge electron transport dominate, since the total τ_E was also increasing. Note that the χ_e results show the same trend as analysis [20] of a less systematic data set, which included a few of the discharges from this scan. For reference, the random uncertainties for the quantities shown in Fig. 3 are 20–30%.

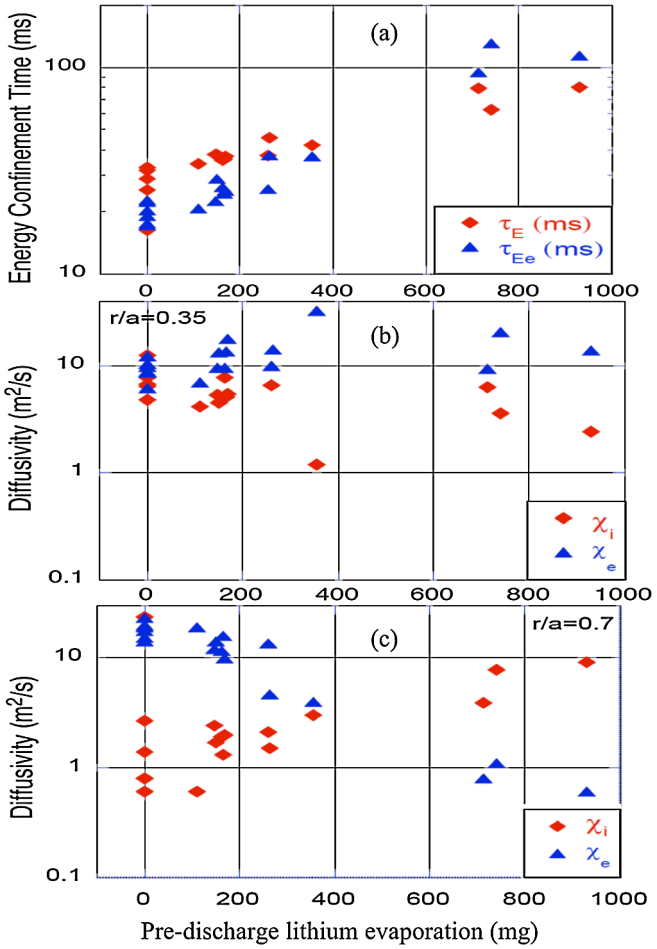

FIG. 3 (color online). Results of core transport analysis as a function of predischarge lithium evaporation: (a) total and electron τ_E, (b) cross-field diffusivities χ_i and χ_e at $r/a = 0.35$, and (c) χ_i and χ_e at $r/a = 0.7$. The three discharges with highest evaporation had P_{NBI} from 2–3 MW.

Many of the discharges in this sequence were also simulated [21] with the 2D edge plasma and neutrals package SOLPS [22], to quantify the change in edge recycling and transport. Profile data were used to constrain the free parameters [23]. Thus, the final particle and thermal diffusivity profiles can be compared to interpret the effect of lithium on cross-field transport coefficients. The simulations showed that both the effective particle diffusion coefficient, D_e^{eff}, and effective electron thermal diffusivity, χ_e^{eff}, from the reference ELMy discharge had a minimum in the vicinity of the steep gradient region from $0.94 < \psi_N < 1$, indicative of the H-mode transport barrier. With increasing discharge number and lithium coatings, both the D_e^{eff} and χ_e^{eff} decreased gradually in the region from $0.8 < \psi_N < 0.94$, until the minimum transport level extended to $\psi_N = 0.8$, the inner domain of the calculation. The D_e^{eff} and χ_e^{eff} values actually increased modestly from $0.94 < \psi_N < 1$, and the D_e^{eff} dropped in the scrape-off layer, i.e., $\psi_N > 1$.

As shown previously [12], the ELM frequency depended on the amount of predischarge lithium deposition. Figure 4(a) shows that the measured ELM frequency during discharges from this sequence decreased with increasing discharge number, i.e., increasing lithium. The transition to ELM-free operation was not quite monotonic, however, in that several discharges with substantial ELM-free periods were followed by ELMy discharges. The diamond data points had edge profiles that were analyzed with an ELM-synchronization method [24,25], whereas the starburst data points were unsuitable to create ELM-synced composite profiles but were included for more insight into the trends. There are several discharges with more than one

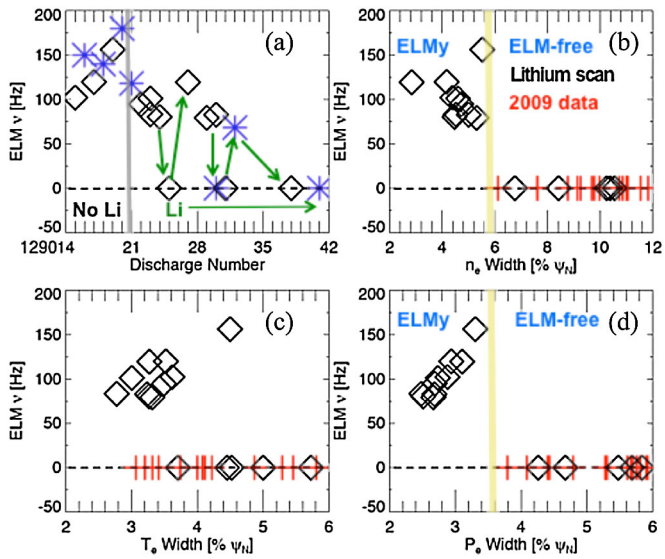

FIG. 4 (color online). (a) Average ELM frequency during the scan; discharges with both ELMy and ELM-free periods of duration >100 ms are shown with multiple data points. (b) ELM frequency dependence on the fitted widths of the (b) n_e, (c) T_e, and (d) P_e profiles.

data point per discharge; in those cases, the edge profiles were analyzed in nonoverlapping time windows of duration ~0.1 sec . This was necessary because the discharges had both an ELMy and an ELM-free phase, or long ELM-free phases with evolving density.

The n_e, T_e, and P_e composite profiles were fitted [24] with a ''standard'' modified hyperbolic tangent (''mtanh'') function [26], which includes both a tanh component and a linear component. The profile changes due to lithium were shown for several lithium evaporation amounts in a recent paper [23]. The ELM frequency from the diamond data points is shown as a function of these pedestal widths in panels 4(b)–4(d). The additional crossed data points were obtained in discharges with heavy lithium wall coatings run in the 2009 campaign, using the same discharge programing and reduced P_{NBI} as in #129038. Clearly, the ELMy and ELM-free data are separated in the n_e and P_e profile widths, with an apparent threshold for suppression. The T_e profile width can be immediately ruled out as an ordering parameter. Since the lithium mainly changes the recycling and the edge fueling, these trends support our hypothesis that the density profile change is central to the ELM suppression.

To summarize, we have shown that many plasma parameters change nearly continuously with increasing lithium coatings. Specifically, the divertor recycling was gradually reduced with increasing lithium wall coatings in NSTX, and the plasma stored energy and normalized τ_E all increased, while the core T_e and P_e profiles became less peaked with increasing lithium wall coatings. The most dramatic changes to the profiles were in the pedestal region, where the n_e and P_e profile widths doubled. Interestingly, the edge T_e gradient remained approximately constant in the H-mode barrier region but increased just inside the top of the pedestal with increasing wall coatings. The ion pressure profile was changed only modestly; hence, the total pressure profile reflected the modification of the electron pressure profile, whose peak gradient and associated bootstrap current moved farther from the separatrix. These profile changes were clearly correlated with the observed gradual suppression of ELMs with increasing lithium, with reduced drive for the kink or peeling mode being the key stabilizing mechanism.

The positive trends documented in this Letter can be used to optimize discharge scenarios, but additional concurrent research is needed to reduce impurity confinement. True ''ELM-free'' scenarios, including the ones in this paper, suffer from impurity accumulation, unless mechanisms to increase impurity transport or reduce the impurity source can be implemented. Lithium itself is not an issue: the lithium concentration in the core remained $<0.1\%$, i.e., negligible [10]. Higher-Z impurities do accumulate, however; the carbon concentration and Z_{eff} in the core increased to $\leq 5\%$, a common feature in high particle confinement ELM-free H-mode. In addition, core radiated power increased monotonically with time, due to an increase in metallic impurity concentrations.

While controlled ELMs triggered by 3D fields have been demonstrated to both reduce the carbon concentration and control radiated power [27], new studies to increase the particle transport continuously with 3D fields, such as demonstrated in DIII-D [28], will be conducted. Our near-term focus is to connect the observed effects back to the amount of predischarge lithium evaporation. The unexpected results have resulted in an increased emphasis on *in situ* plasma surface diagnostics [29] to understand the complex lithium-carbon interactions, as well as several new directions in lithium coating technologies.

This research was supported in part by the U.S. Department of Energy under Contracts No. DE-AC05-00OR22725, No. DE-AC02-09CH11466, No. DE-FC02-04ER54698, No. DE-FG03-99ER54527, No. DE-FG02-99ER54524, and No. DE-AC52-07NA27344.

[1] J. Winter, Plasma Phys. Controlled Fusion **36**, B263 (1994).
[2] J. Snipes, E. S. Marmar, and J. L. Terry, J. Nucl. Mater. **196–198**, 686 (1992).
[3] D. K. Mansfield *et al.*, Nucl. Fusion **41**, 1823 (2001).
[4] R. Majeski *et al.*, Phys. Rev. Lett. **97**, 075002 (2006).
[5] M. Apicella *et al.*, J. Nucl. Mater. **363–365**, 1346 (2007).
[6] J. Sánchez *et al.*, J. Nucl. Mater. **390–391**, 852 (2009).
[7] J. Brooks *et al.*, J. Nucl. Mater. **337–339**, 1053 (2005).
[8] H. W. Kugel *et al.*, J. Nucl. Mater. **363–365**, 791 (2007).
[9] H. W. Kugel *et al.*, Phys. Plasmas **15**, 056118 (2008).
[10] M. G. Bell *et al.*, Plasma Phys. Controlled Fusion **51**, 124054 (2009).
[11] H. W. Kugel *et al.*, J. Nucl. Mater. **390–391**, 1000 (2009).
[12] D. K. Mansfield *et al.*, J. Nucl. Mater. **390–391**, 764 (2009).
[13] R. Maingi *et al.*, Phys. Rev. Lett. **103**, 075001 (2009).
[14] R. Maingi *et al.*, Nucl. Fusion **51**, 063036 (2011).
[15] R. Maingi *et al.*, Nucl. Fusion **45**, 264 (2005).
[16] S. A. Sabbagh *et al.*, Nucl. Fusion **41**, 1601 (2001).
[17] S. M. Kaye, M. Greenwald, and U. Stroth, Nucl. Fusion **37**, 1303 (1997).
[18] R. J. Hawryluk, in *Physics of Plasmas Close to Thermonuclear Conditions* (Pergamon, Oxford, 1980), Vol. 1, p. 19.
[19] L. L. Lao *et al.*, Nucl. Fusion **25**, 1611 (1985).
[20] S. Ding *et al.*, Plasma Phys. Controlled Fusion **52**, 015001 (2010).
[21] J. M. Canik *et al.*, J. Nucl. Mater. (to be published).
[22] R. Schneider, Contrib. Plasma Phys. **46**, 3 (2006).
[23] J. M. Canik *et al.*, Phys. Plasmas **18**, 056118 (2011).
[24] D. P. Boyle *et al.*, Plasma Phys. Controlled Fusion **53**, 105011 (2011).
[25] T. H. Osborne *et al.*, J. Phys. Conf. Ser. **123**, 012014 (2008).
[26] R. J. Groebner and T. H. Osborne, Phys. Plasmas **5**, 1800 (1998).
[27] J. M. Canik *et al.*, Phys. Rev. Lett. **104**, 045001 (2010).
[28] T. E. Evans *et al.*, Nature Phys. **2**, 419 (2006).
[29] C. H. Skinner *et al.*, J. Nucl. Mater. (to be published).